Earthquakes and Structures, *Vol. 9, No. 1 (2015) 233-256*
DOI: http://dx.doi.org/10.12989/eas.2015.9.1.233

Seismic behavior of reinforced concrete exterior beam-column joints strengthened by ferrocement composites

Bo Li[1], Eddie Siu-shu Lam[*1], Bo Wu[2] and Ya-yong Wang[3]

[1]*Department. of Civil & Environmental Engineering, The Hong Kong Polytechnic University, Hong Kong*
[2]*School of Architectural and Civil Engineering, South China University of Technology, Guangzhou, China*
[3]*Institute of Earthquake Engineering, China Academy of Building Research, Beijing, China*

(Received October 6, 2014, Revised February 7, 2015, Accepted February 12, 2015)

Abstract. This paper presents an experimental study to assess the effectiveness of using ferrocement to strengthen deficient beam-column joints. Ferrocement is proposed to protect the joint region through replacing concrete cover. Six exterior beam-column joints, including two control specimens and four strengthened specimens, are prepared and tested under constant axial load and quasi-static cyclic loading. Two levels of axial load on column (0.2*fc'Ag* and 0.4*fc'Ag*) and two types of skeletal reinforcements in ferrocement (grid reinforcements and diagonal reinforcements) are considered as test variables. Experimental results have indicated that ferrocement as a composite material can enhance the seismic performance of deficient beam-column joints in terms of peak horizontal load, energy dissipation, stiffness and joint shear strength. Shear distortions within the joints are significantly reduced for the strengthened specimens. High axial load (0.4*fc'Ag*) has a detrimental effect on peak horizontal load for both control and ferrocement-strengthened specimens. Specimens strengthened by ferrocement with two types of skeletal reinforcements perform similarly. Finally, a method is proposed to predict shear strength of beam-column joints strengthened by ferrocement.

Keywords: reinforced concrete; beam-column joints; strengthening; ferrocement; composite; cyclic behavior

1. Introduction

In regions with low to moderate seismic risk, such as Hong Kong, seismic design and detailing may not be considered for reinforced concrete (RC) structures. Structures are normally designed based on gravity loads and wind loads. It is common that beam-column joints in such structures are with inadequate transverse reinforcement. These joints have been proved to be critical members when subjecting to seismic attack. In fact, performance of beam-column joints significantly affects behavior of frame (Costa *et al*. 2013). Failure of beam-column joints may cause catastrophic collapse of buildings (Kam *et al*. 2011). Thus, proper strengthening is required to enhance the seismic performance of beam-column joints without seismic provision.

In the past decades, numerous strengthening methods have been proposed for non-seismically

*Corresponding author, Associate Professor, E-mail: cesslam@polyu.edu.hk

http://www.techno-press.org/journals/eas&subpage=7 ISSN: 2092-7614 (Print), 2092-7622 (Online)

designed beam-column joints. With excellent compatibility with the original structure, concrete jacketing was proved to be effective for strengthening beam-column joints (Alcocer and Jirsa 1993, Hakuto *et al.* 2000). As an alternative mean of concrete jacketing, shotcrete was also employed to strengthen exterior beam-column joints (Tsonos 2010). It has been demonstrated that concrete jacketing is effective to improve strength and ductility of beam-column joints. However, application of concrete jacketing is limited due to its labor intensive, complex and space occupation. Steel jacketing was another strengthening method for beam-column joints. Ghobarah *et al.* (1997) upgraded non-ductile RC frame connections using corrugated steel jacketing. Additional protections were required to prevent corrosion and to resist fire. Fiber reinforced polymer (FRP) has gained popularity for structural strengthening because of its excellent characteristics in high strength/weight ratio, corrosion resistance, ease of application. Carbon or glass FRPs with various wrapping schemes have been widely used to upgrade beam-column joints (Ghobarah and Said 2002, Antonopoulos and Triantafillou 2003, Prota *et al.* 2004, Pantelides *et al.* 2008, Li and Chua 2009, Al-Salloum *et al.* 2010, Akguzel and Pampanin 2010, Sezen 2012). Significant improvements in strength and ductility were attained for FRP-strengthened beam-column joints. FRP strengthening method eliminates many of limitations of concrete jacketing, such as labor intensive. However, application of FRP wrapping is limited by, e.g., instability of bonding on a wet substrate, poor fire resistance, low reversibility, and lack of vapor permeability (Babaeidarabad *et al.* 2014). Furthermore, it requires advance treatment for bonding FRP on concrete surface with some degrees of spalling. Anchorage of FRP is another critical issue for achieving strengthening as debonding has been found to dominate the behavior of FRP reinforcements (Antonopoulos and Triantafillou 2003). Application of FRP wrapping is subjected to constructional limitations due to obstruction of beams or slabs (Karayannis and Sirkelis 2008). To overcome these shortcomings, cement-based composites have been proposed to strengthen beam-column joints.

Shannag and Alhassan (2005) upgraded interior beam-column joints with 25 mm-thick jackets made of high performance fiber reinforced concrete matrix. Substantial enhancement in strength, energy dissipation and stiffness degradation was achieved for the strengthened beam-column joints. Karayannis *et al.* (2008) experimentally investigated the seismic behavior of beam-column joints rehabilitated by locally applied reinforced mortar jacketing. Experimental results showed that layered reinforced mortar jacketing improved seismic behavior and damage states. Al-Salloum *et al.* (2011) investigated the effectiveness of textile-reinforced mortars (TRM) for strengthening beam-column joints and compared with FRP-strengthened beam-column joints. It was found that TRM-strengthened joint exhibited strength and ductility comparable to FRP-strengthened joint.

In this study, ferrocement is proposed to strengthen deficient beam-column joints as alternative cement-based composites. Ferrocement is a type of composite material consisting of cementitious mortar uniformly reinforced with one or more layers of wire mesh. Sometimes, skeletal reinforcements are provided within ferrocement (Naaman 2000). With advantages in homogeneous and bidirectional properties, ferrocement has been used for strengthening RC beams and columns. Paramasivam *et al.* (1998) applied ferrocement laminates for flexural strengthening of RC beams. Mourad and Shannag (2012), Ho *et al.* (2013) investigated axial compression behavior of square and circular RC columns strengthened by ferrocement respectively. Takiguchi and Abdullah (2001), Kazemi and Morshed (2005) performed experimental studies on seismic performance of columns strengthened by ferrocement jackets. It has been demonstrated that ferrocement composites improved the performance of structural members. On the other hand, application of ferrocement for strengthening beam-column joints has not been well studied. Among others, Sheela and Geetha (2012) compared the behavior of exterior beam-column joints strengthened by ferrocement and FRP. Ferrocement-strengthened joint showed less stiffness degradation and better cost-effectiveness as compared with FRP-strengthened joint. Ravichandran and Jeyasehar (2012) strengthened exterior beam-column joints through bonding ferrocement laminate on concrete substrate. Test results of eight full-scale joints indicated externally bonding ferrocement was effective to improve the seismic behavior of beam-column joints. Kannan *et al.* (2013) investigated the seismic performance of non-seismically designed beam-column joints strengthened by ferrocement jackets. Ferrocement was effective to improve seismic behavior in terms of ultimate load carrying capacity, ultimate deflection, energy dissipation and ductility. Moreover, use of diagonal reinforcements in joint region has been proved to be effective to enhance joint behavior and reduce damage level (Chalioris *et al.* 2008, Asha and Sundararajan 2014, Rajagopal *et al.* 2014). Recently, the authors of this paper have successfully rehabilitated RC interior beam-column joints by ferrocement jackets (Li *et al.* 2013). This study has extended application of ferrocement for strengthening exterior beam-column joints through replacing concrete cover.

The objective of this study is to assess the effectiveness of using ferrocement to strengthen RC exterior beam-column joints. Six exterior beam-column joints were prepared and tested under constant axial load and reversed horizontal loading. Two strengthening schemes with different skeletal reinforcements in ferrocement are examined. Influence of axial load on the seismic performance of exterior beam-column joints with and without strengthening is compared. Finally, a method is proposed to predict the shear strength of beam-column joints strengthened by ferrocement.

2. Experimental program

2.1 Specimens

Six 2/3-scale exterior beam-column joints, including two control specimens (identified as EJC1 and EJC2) and four strengthened specimens (identified as EJS1, EJS2, EJS3 and EJS4) were prepared. They are divided into two groups according to the amount of applied axial load. Specimens EJC1, EJS1 and EJS2 are in high axial load group and specimens EJC2, EJS3 and EJS4 are in low axial load group. Allocation of specimens is provided in Table 1.

All specimens have identical geometry and reinforcement details as shown in Fig. 1. The specimens have beam section of 250 mm×400 mm and column section of 300 mm×300 mm. Lengths of the beam and the column are 1,200 mm and 2,385 mm, respectively. Reinforcement detail of beam comprises four T12 high yield deformed reinforcements in both tension zone and compression zone or has 1.6% longitudinal reinforcement ratio. Column has twelve T12 high yield deformed reinforcements (2.7% longitudinal reinforcement ratio) distributed around the perimeter uniformly. Single stirrup using R8 mild steel at 150 mm spacing is adopted as transverse reinforcements in both beams and columns. Spacing of transverse reinforcement is reduced to 100 mm at the 400 mm ends. All specimens are designed without transverse reinforcement in the joints. Both tension and compression reinforcements are bend into the joint. Anchorage for bottom reinforcements is based on standard hook with at least 8ϕ extension. Here, ϕ is the diameter of longitudinal reinforcement. Full anchorage length is provided for the top reinforcements according to CopConcrete (1987). Anchorage detail within the joint is also shown in Fig. 1. For simplicity,

Table 1 Details of the specimens

Group	Spec.	Descriptions	Axial load ratio
High axial load	EJC1	Control specimen without strengthening	0.4
	EJS1	Specimen strengthened by ferrocement with grid skeletal reinforcements	0.4
	EJS2	Specimen strengthened by ferrocement with diagonal skeletal reinforcements	0.4
Low axial load	EJC2	Control specimen without strengthening	0.2
	EJS3	Specimen strengthened by ferrocement with grid skeletal reinforcements	0.2
	EJS4	Specimen strengthened by ferrocement with diagonal skeletal reinforcements	0.2

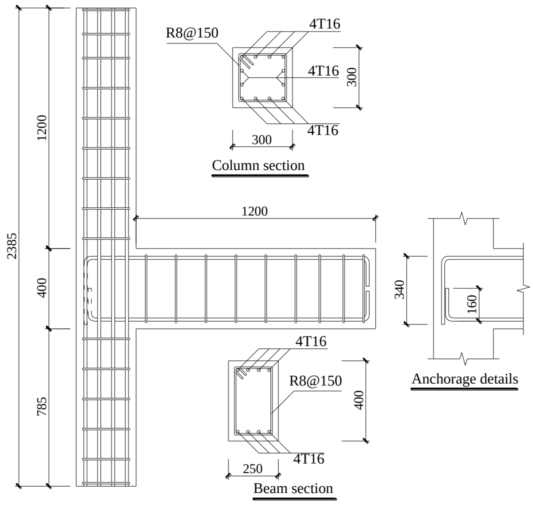

Fig. 1 Dimensions and reinforcement details of the specimens (unit: mm)

transverse beam and slab are not modeled for beam-column joints. This represents a joint without transverse beam or with small-size transverse beams. In the other studies, beam-column joints were connected to large-size transverse beams and may have additional confinement (Ehsani and Wight 1985).

2.2 Strengthening method

Two strengthening schemes using ferrocement composites with different skeletal reinforcements are proposed to improve the seismic performance of deficient exterior beam-column joints. Ferrocement composites are proposed to replace concrete cover and to wrap the joint. To provide adequate anchorage, ferrocement composites are extended to the beam and the columns. Length of ferrocement jacket is determined according to previous study (Li *et al.* 2014). Skeletal reinforcements are provided within the ferrocement composites in the forms of grid reinforcements and diagonal reinforcements. Details of two strengthening schemes are introduced in the following section.

Two strengthening schemes, named Scheme A and Scheme B, differentiated in forms of skeletal reinforcements and wire mesh, are shown in Fig. 2. For Scheme A, the combined use of

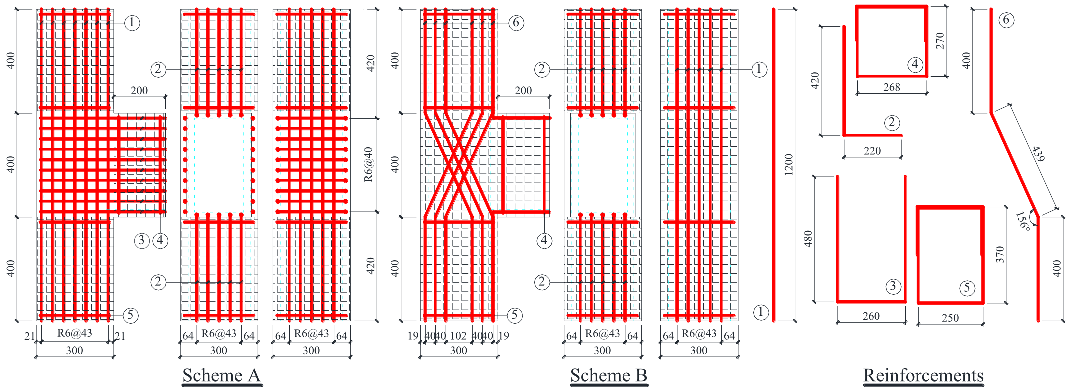

Fig. 2 Strengthening schemes using ferrocement composites (unit: mm)

(a) (b)

Fig. 3 Photos of exterior beam-column joints wrapped by (a) Scheme A and (b) Scheme B

U-shaped steel bars in the beam and vertical steel bars in the column forms the reinforcement grids at the joint core. L-shaped steel bars are also installed at the beam-column interfaces. Ends of U-shaped bars, L-shaped bars and vertical bars are wrapped by two layers of wire mesh at the beam and the columns as shown in Fig. 3(a). Stirrups are only provided at beam-column interfaces and ends of strengthening area with the purpose of fixing skeletal steel bars. In Scheme B, vertical steel bars are replaced by diagonal steel bars in the joint. The amount of skeletal reinforcements in Scheme B (1.64% volumetric ratio in ferrocement) is significantly less than that in Scheme A (2.49% volumetric ratio in ferrocement). Wrapping of wire mesh at ends of the beam and the columns is also provided. Additional U-shaped wire mesh is provided to wrap around the joint area in Scheme B as shown in Fig. 3(b). Finally, a non-shrinkage, flowable mortar is used to cast the ferrocement composites. Thickness of ferrocement composites is 30 mm.

Procedure for strengthening of exterior beam-column joints using the proposed method is illustrated in Fig. 4. It consists of the following steps: (a) Concrete cover in the joint region was first removed (e.g., consider due to spalling of concrete). Surface of the strengthening area in the joint was properly roughened by a jet hammer and cleaned by compressed air. This improves the bonding between ferrocement composites and concrete substrate; (b) Small-diameter skeletal reinforcements and wire mesh properly cut and folding were installed in the joint; (c) Formwork was setup and properly sealed to prevent leakage of mortar; (d) After concrete surface was slightly wetted, flowable mortar was poured into the formwork gradually; and (e) Proper curing was provided with continuous moisture condition before demolding.

(a) Treatment surface

(b) Installation of wire mesh and skeletal reinforcements

(c) Set up of formwork

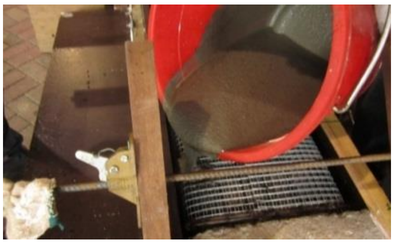

(d) Apply mortar

(e) Strengthened specimen

Fig. 4 Strengthening procedure for beam-column joints using the propsed method

Table 2 Material properties of concrete and mortar

Specimen		EJC1	EJS1	EJS2	EJC2	EJS3	EJS4
Concrete	Strength (MPa)	52.8	52.8	54.3	50.4	54.7	51.7
	E-value (Gpa)	30.0	30.0	30.0	32.7	32.7	32.7
Mortar	Strength (Mpa)	--	85.6	75.9	--	71.9	77.4
	E-value (Gpa)	--	32.5	28.4	--	27.3	23.7

Table 3 Material properties of reinforcements and wire mesh

Reinforcement	Yield strength (MPa)	Ultimate strength (MPa)	E-value (GPa)
T16	530.7	645.3	202.3
R8	374.7	521.8	217.7
R6	350.0	420.0	205.0
Wire mesh	--	537.0 (Long.) 508.0 (Trans.)	--

2.3 Materials

Ready-mixed concrete was adopted for constructing the specimens. Specimens EJC1, EJS1 and EJS2 were cast in the first batch while specimens EJC2, EJS3 and EJS4 were cast in second batch. Concrete strength was measured on the day of testing for each specimen from compressive test on three test cubes. Young's modulus of concrete was estimated at the 28th day. Strength and Young's modulus of mortar were assessed on the day of testing for each specimen. Material properties of concrete and mortar are summarized in Table 2. T12 high yield deformed steel bars are used as longitudinal reinforcements. R8 and R6 mild steel bars are adopted as transverse reinforcements and skeletal reinforcements, respectively. Square welded wire mesh used in ferrocement has a diameter of 1.1 mm and center-to-center spacing of 12.5 mm in both directions. Material properties for reinforcements and wire mesh are shown in Table 3.

2.4 Test setup and instrumentations

Exterior beam-column joints are tested using a multi-purposes testing system in The Hong Kong Polytechnic University as shown in Fig. 5(a). This system has axial capacity of 10,000 kN in vertical direction and 1,500 kN in horizontal pull-push direction. Bottom end of the column is connected to a strong floor through a hinge which restrains horizontal and vertical movements. Upper column is hinged to two actuators in vertical and horizontal directions, respectively. The vertical actuator for applying axial load is free to move under horizontal displacement. Axial load on column is kept constant and remains vertical throughout the test. Thus, P-Δ effect is included in the test as shown in deflected shape of the specimen in Fig. 5(b). End of beam is restrained against vertical displacement only.

(a)

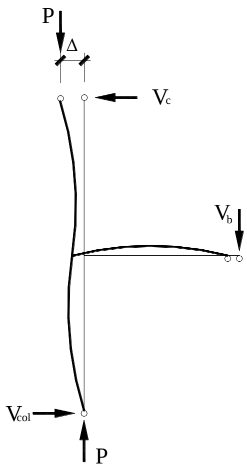

(b)

Fig. 5 Test setup and deflected shape for exterior beam-column joint

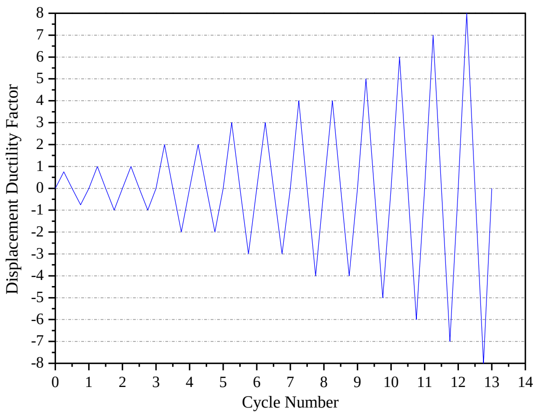

Fig. 6 Loading sequence for specimens

Structural response of beam-column joints was recorded by load cells, linear variable displacement transducers (LVDTs) and strain gauges. Axial loads and horizontal loads were monitored during the test by the load cells provided by the testing machine. Displacements at specific locations were measured by LVDTs and were used for monitoring local and global deformations. Strains of reinforcements were collected at critical locations of the beam, the column and the joint region using electrical resistance strain gauges. At each location, a pair of strain gauge was used to monitor the strain.

2.5 Loading sequence

Loading sequence consists of axial load on the column and reversed horizontal load on the upper column. Two levels of axial load ($0.2f_c^{'}A_g$ and $0.4f_c^{'}A_g$) were applied to investigate the influence of axial load on the seismic performance of beam-column joints with and without strengthening. The adopted axial loads are based on the common loading conditions of columns in the buildings in Hong Kong. Su and Wong (2007) demonstrated that high axial load can be attained at the lower story of buildings. Similar level of high axial load was also adopted by Li and Chua (2009), Hassan and Moehle (2012). Low axial load is determined based on gravity. Axial load was kept constant for each specimen during the test. Horizontal load was applied based on displacement ductility (equal to applied displacement over yield displacement). Yield displacement was determined based on flexural capacity of the beam (Li *et al.* 2013). Due to the influence of P-Δ effect, yield displacement of specimens under different axial loads was different. Subsequently, horizontal load was applied under progressive increase in displacement ductility factor. Each cycle at constant displacement ductility factor was repeated twice. Same loading sequence was adopted for the strengthened specimens under the same axial load. As cyclic demands for a structure depend on a large number of variables, a unique loading history is normally to be a compromise. The adopted loading sequence is a typical one to determine structural performance under arbitrary seismic excitations (Karayannis and Sirkelis 2008). Loading sequence for specimens under different axial load is shown in Fig. 6.

3. Experimental results

3.1 Observations and failure modes

3.1.1 Control specimens

Crack patterns of control specimens EJC1 and EJC2 are shown in Fig. 7(a) and Fig. 7(b), respectively. Flexural cracks were first observed in the beams. Cracks in the joints occurred at drift ratio of 0.94% and 0.72% for specimens EJC1 and EJC2, respectively. Presence of high axial load delayed initial cracking in the joint. Since no transverse reinforcement was provided in the joints, cracks in the joints developed rapidly while cracks in the beams ceased to develop. Diagonal cracks in specimen EJC1 were steeper than those in specimen EJC2. This reflected different stress states which were affected by high axial load. As the drift ratio increased, cracks in the joints propagated to the columns. However, flexural crack was not observed in the columns. This may be attributed to applied axial load on column which reduced axial tension strain of concrete. Opening and closing of cracks in the joints resulted in spalling of concrete at drift ratio of 1.99% and 2.16% for specimens EJC1 and EJC2, respectively. It indicates that high axial load aggregates cracking in

(a) (b)

Fig. 7 Crack patterns of control specimens (a) EJC1 and (b) EJC2 after test

the joints. With further increase in drift ratio, a wedge-shaped concrete was developed in the joints close to the free edge and was nearly separated from the joints. It demonstrated that concrete in the joints without adequate confinement was prone to spalling off. Generally, both control specimens EJC1 and EJC2 failed in joint shear mode, which confirmed the vulnerability of beam-column joints without seismic detailing.

3.1.2 Strengthened specimens

Crack patterns of strengthened specimens are shown in Fig. 8. Flexural cracks were first observed at beam-column interfaces and at un-strengthened area of the beams. As the drift ratio increased, cracks at beam-column interfaces propagated into the joints. Cracks were observed in the joints at drift ratio of 0.94% for strengthened specimens under high axial load and at drift ratio of 1.44% for those under low axial load. Strengthening method could delay cracking in the joints for specimens under low axial load. Simultaneously, more cracks were observed in un-strengthened area of the beams. Subsequently, cracks developed in two different patterns.

• Type I (specimen EJS1): Cracks in the joint and interface ceased to develop while inclined cracks in un-strengthened area of the beam developed rapidly. This highlighted the use of U-shaped skeletal reinforcements in ferrocement composites to enhance moment capacity at beam-column interface. As a result, beam-column interface was prevented from cracking and strain penetration into the joint was reduced. Two large inclined cracks developed in un-strengthened area of the beam led to the failure of specimen EJS1 in beam shear as shown in Fig. 8(a). It demonstrates that the use of ferrocement is effective to protect the joint from damage. However, attention should be paid on prevention of brittle shear failure in the beam after strengthening of the joint. Generally, specimen EJS1 failed in shear mode in un-strengthened area of the beam.

• Type II (specimens EJS2, EJS3 and EJS4): Cracks developed at beam-column interfaces with obvious increase in crack width. Due to strain penetration, cracking in the joints occurred with the opening and closing of the interfacial cracks. However, ferrocement composites with skeletal reinforcements restrained further development of cracks in the joints. Here, shear capacity of beam was enhanced for specimen EJS3 so as to avoid beam shear failure which occurred in specimen EJS1. It helped to check whether failure could be shifted to a ductile manner, i.e. beam flexural. During the test, no delamination between ferrocement composites and concrete substrate was observed. Finally, failure of specimens EJS2, EJS3 and EJS4focused at beam-column interfaces

(a) (b) (c) (d)

Fig. 8 Crack patterns of specimens (a) EJS1, (b) EJS2, (c) EJS3, and (b) EJS4 after test

with extension to joint regions as shown in Fig. 8(b) to (d).

Comparatively, both strengthening schemes effectively restrained the joint regions without transverse reinforcement. Scheme A with more skeletal reinforcements had better ability on crack control. For instance, specimens with diagonal skeletal reinforcements have wider cracks in the joint as compared with those with grid skeletal reinforcements. Strengthened specimens under high axial load exhibited less cracks as compared with those under low axial load. One of the reasons is that specimens under low axial load achieved a larger horizontal displacement. After the formation of interfacial cracks for the specimens strengthened by the same scheme, high axial load is able to suppress the development of cracks in the joints.

3.2 Hysteretic behavior

Hysteretic behavior of beam-column joints is examined in terms of horizontal load and displacement. The relationships of horizontal load versus displacement at upper column for the specimens are illustrated in Fig. 9. Summary of the test results is shown in Table 4. Envelops of hysteretic loops for all specimens are plotted in Fig. 10.

Peak horizontal loads of strengthened specimens are enhanced as compared with that of control specimens under both high and low axial loads. For specimens under high axial load, peak horizontal loads are enhanced by 30.6% and 28.0% for specimens EJS1 and EJS2 respectively as compared with that of specimen EJC1. Specimen EJS1 with more skeletal reinforcements in ferrocement composites possesses higher peak horizontal load. Use of U-shaped steel bars in Scheme A is effective for preventing formation of critical section at beam-column interface and causing strain penetration to the joint. This has been proved to be beneficial for reducing strength degradation in the joints. For specimens under low axial load, peak horizontal loads are enhanced by 16.3% and 12.5% for specimens EJS3 and EJS4 respectively as compared with that of specimen EJC2. Similarly, specimen EJS3 with more skeletal reinforcements in ferrocement composites has higher peak horizontal load. Generally, specimens with grid reinforcements exhibit slightly better performance in achieving higher peak horizontal load as compared with specimens with diagonal reinforcements. When comparing the enhancement ratio of peak horizontal load for specimens under low and high axial loads, the proposed strengthening method is more efficient for the specimens under high axial load.

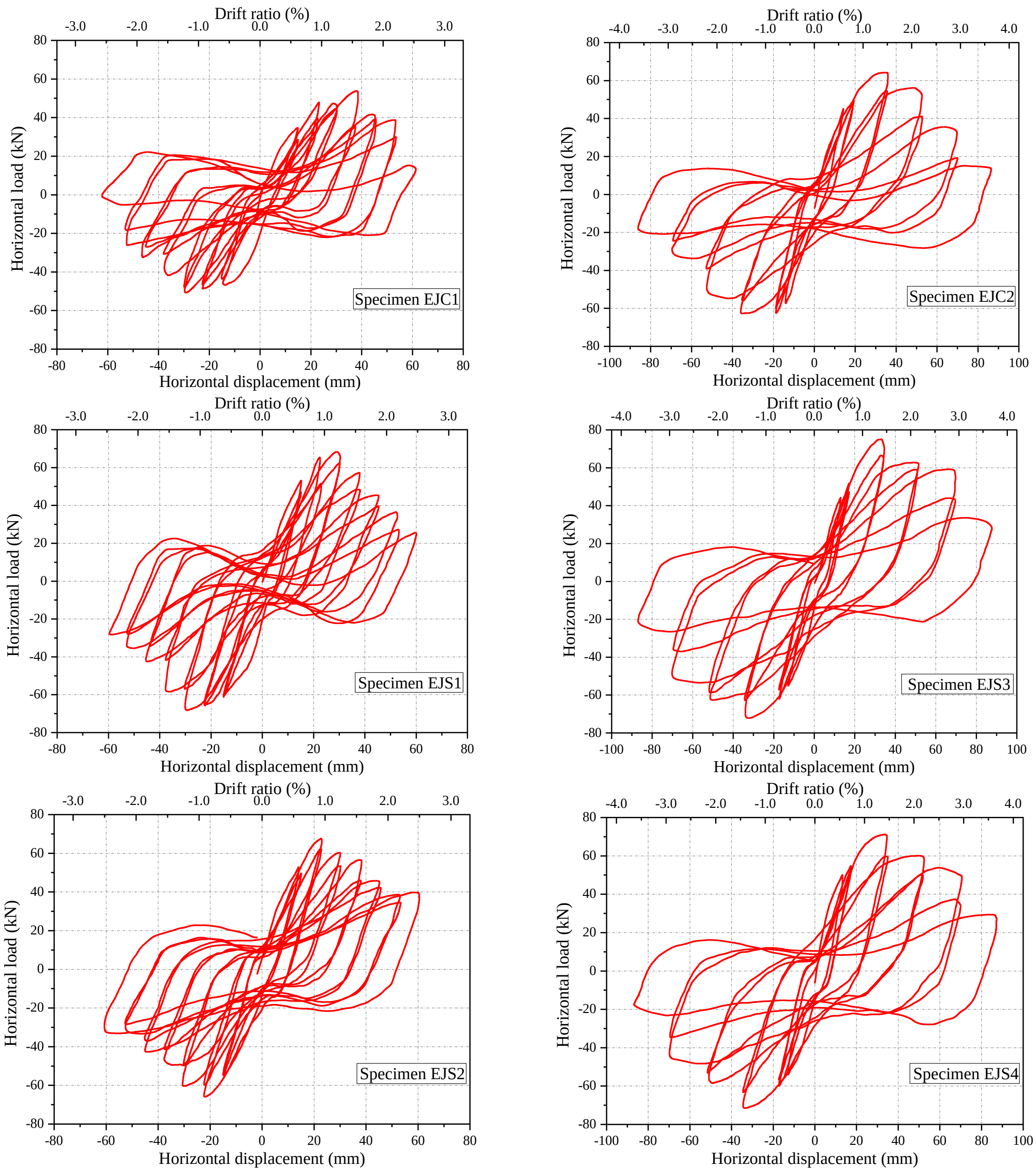

Fig. 9 Relationship of horizontal load versus displacement for the specimens

Deformation ability of beam-column joints is examined in term of displacement at peak horizontal load. Displacement at peak horizontal load is slightly decreased for strengthened specimens under high axial load as compared with that of control specimen. This is attributed to the increase in stiffness as well as concentration of failure in the strengthened specimens. This induces deformation of the specimen to concentrate at the weakest location. For instance, failure in strengthened specimens concentrates at un-strengthened area of beam for specimen EJS1 and at beam-column interface for specimen EJS2. For specimens under low axial load, peak horizontal

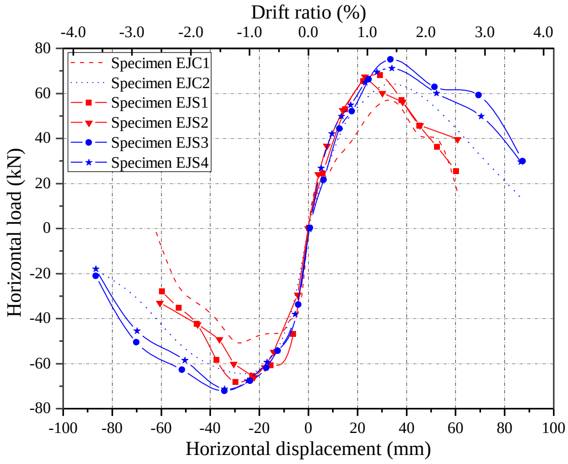

Fig. 10 Envelops of hysteretic loops for the specimens

Table 4 Summary of test results for the specimens

Spec.	Axial load ratio	Peak horizontal load		Joint shear strength		Failure modes
		Peak load (kN)	Enhancement ratio	Joint strength (MPa)	Enhancement ratio	
EJC1	0.4	52.28	1	$0.75\sqrt{f_c'}$	1	Joint shear
EJS1	0.4	68.29	1.306	$0.87\sqrt{f_c'}$	1.159	Beam shear
EJS2	0.4	66.92	1.280	$0.79\sqrt{f_c'}$	1.055	Beam-column Interface
EJC2	0.2	63.40	1	$0.77\sqrt{f_c'}$	1	Joint shear
EJS3	0.2	73.72	1.163	$0.82\sqrt{f_c'}$	1.058	Beam-column Interface
EJS4	0.2	71.31	1.125	$0.83\sqrt{f_c'}$	1.068	Beam-column Interface

loads are achieved at the same displacement. Effect of strengthening method on deformation capacities of beam-column joints is not significant. Concentration of failure also leads to the similar post-peak behavior for the specimens under high or low axial load (as shown in Fig. 10). In addition, as P-Δ effect introduces additional force to the joint, specimens under high axial load are subjected to larger additional forces as compared with the one under low axial load at the same horizontal displacement. Deformation abilities of specimens under high axial load are smaller than that of specimens under low axial load.

3.3 Energy dissipation

Energy dissipation is calculated from the area of hysteretic loops. Fig. 11 compares cumulative energy dissipation against drift ratio for the specimens under both high and low axial loads. All strengthened specimens exhibit improved energy dissipation. For specimens under high axial load as shown in Fig. 11(a), energy dissipation capacities of strengthened specimens are higher than that of control specimen when the drift ratio reaches 0.93%. Both strengthened specimens have similar energy dissipation capacities until drift ratio reaches 2.0%. Shear failure of beam in specimen EJS1 reduces energy dissipation at the final stage of loading. For the specimens under

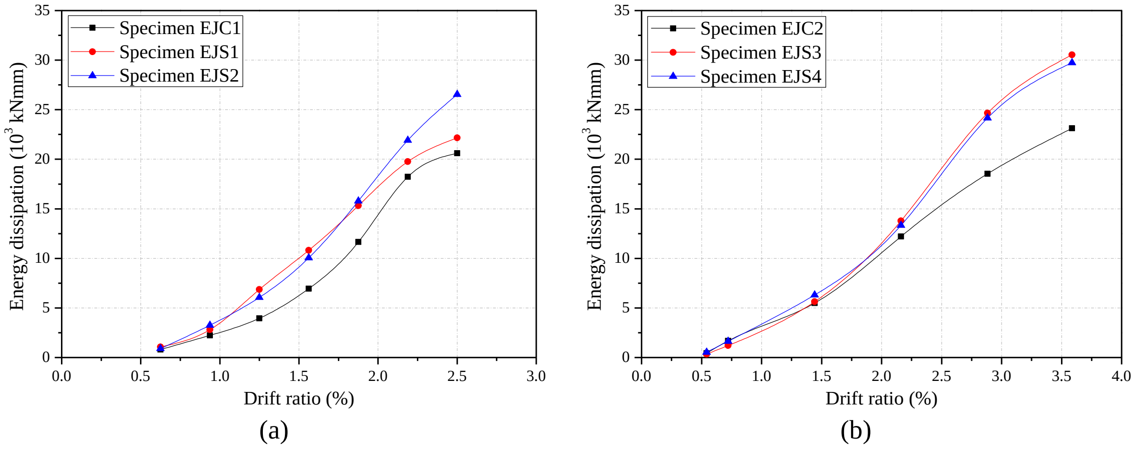

Fig. 11 Comparison of energy dissipation of the specimens under (a) high axial load and (b) low axial load

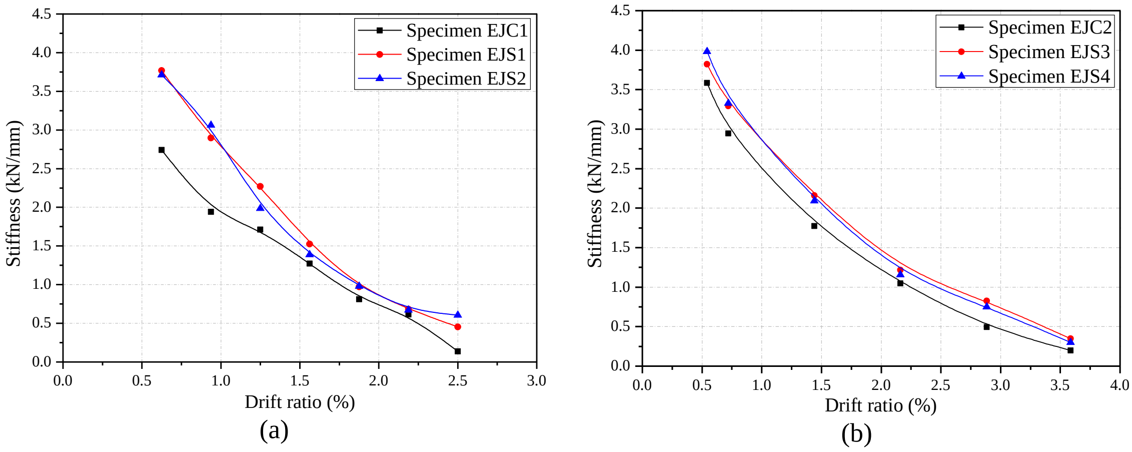

Fig. 12 Stiffness degradation for the specimens under (a) high axial load and (b) low axial load

low axial load as shown in Fig. 11(b), effect of strengthening on energy dissipation is triggered at drift ratio of 2.0%. Similarly, both strengthened specimens under low axial load show nearly the same energy dissipation capacities. Specimens under high axial load have higher energy dissipation capacities as compared with those under low axial load at the same drift ratio. However, specimens under low axial load can continuously dissipate energy to a large drift ratio and have higher energy dissipation.

3.4 Stiffness degradation

Stiffness at each cycle determined from slope of a line passing peak-to-peak points at each hysteretic loop is given in Fig. 12. After strengthening, specimens under both high and low axial loads show higher stiffness at each drift ratio as compared with the control specimens. Enhancement in initial stiffness of strengthened specimens under high axial load is larger than that of strengthened specimens under low axial load. However, high axial load has detrimental effect on stiffness degradation since stiffness of specimens under high axial load decrease rapidly. Strengthened specimens under low axial load exhibit similar stiffness degradation rate as compared with control specimen. Under high and low axial loads, both strengthened specimens with grid and diagonal skeletal reinforcements have almost the same stiffness degradation. In general, the proposed strengthening method is able to enhance the stiffness of beam-column joints.

3.5 Strain of reinforcements

Strain of reinforcement is affected by cracking pattern of the specimen. Since all specimens experience cracking at beam-column interfaces, strains of reinforcements at such location are compared to evaluate shear force applied to the joint. Thus, strains of longitudinal reinforcements in the beam close to beam-column interfaces against horizontal displacement for all specimens are compared in Fig. 13. The data are collected by taking average of the readings of two strain gauges at 25 mm away from column face. At the initial stage of loading, similar strains of reinforcements at beam-column interfaces are obtained from all specimens. For specimens under high axial load, longitudinal reinforcements in control specimen yield at beam-column interface at around 30 mm horizontal displacement and increase rapidly afterwards. On the contrary, strains of longitudinal reinforcements in strengthened specimens are without significant variation. For instance, upper longitudinal reinforcements at interface in specimen EJS1 exhibit smaller strains due to failure in the beam. For specimens under low axial load, reinforcements at interface for strengthened specimens exhibit lower strains as compared with those for control specimen. As failure of strengthened specimens occurred at beam-column interface, strains of longitudinal reinforcements

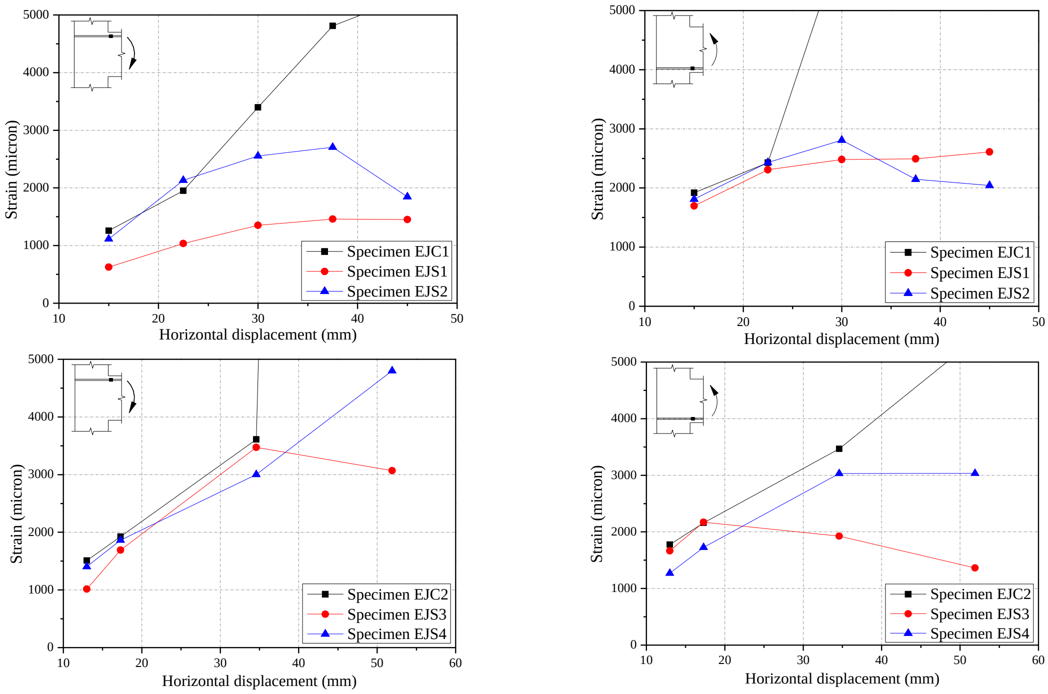

Fig. 13 Strains of longitudinal reinforcements of beam at beam-column interfaces

reach yielding value. Generally, strains of reinforcements at beam-column interface are reduced in strengthened specimens under both high and low axial loads. However, reduction on reinforcement strains between control and strengthened specimens under low axial load are smaller than that under high axial load. This indicates the strengthening method is more effective for the joints under high axial load.

3.6 Shear distortion

Shear distortion is computed based on measurements of a pair of diagonal LVDTs installed in the joint. It is the sum of horizontal and vertical shear distortions as shown in Fig. 14. Shear distortion can be calculated using Eq. (1)

$$\gamma_j = \gamma_1 + \gamma_2 = \frac{\sqrt{l_h^2 + l_v^2}}{2 l_h l_v}(\delta_1 - \delta_2) \tag{1}$$

where γ_j is the shear distortion of the joint; γ_1 and γ_2 are the horizontal and vertical shear

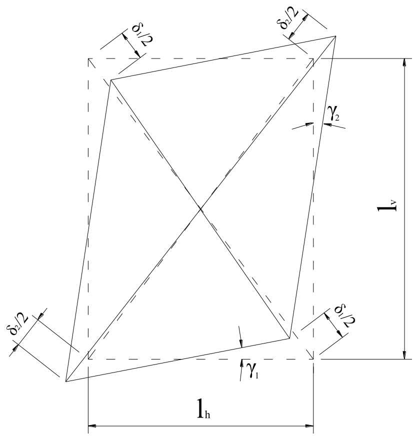

Fig. 14 Shear distortion of joint core

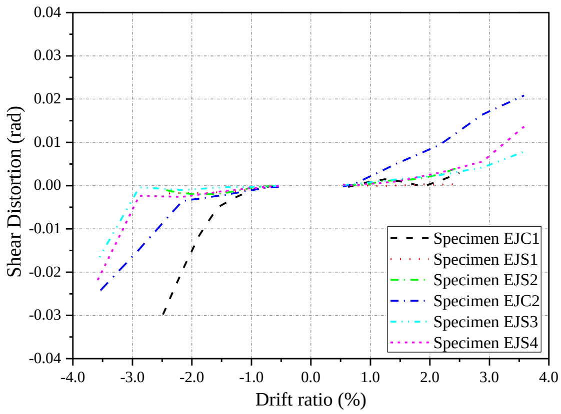

Fig. 15 Comparison of shear distortion against drift ratio for the specimens

deformation angles, respectively; l_h and l_v are the horizontal and vertical distances of LVDTs installed in the joint, respectively; δ_1 and δ_2 are the measurements of diagonal LVDTs. Here, "+"represents for lengthening and "-" represents for shortening. Fig. 15 shows the comparison of shear distortion against drift ratio for all specimens. Shear distortions of control specimens under both high and low axial loads increase as drift ratio increases. Beam-column joints without transverse reinforcement are prone to deform at early stage of loading. After strengthening, shear distortions of strengthened specimens under both high and low axial loads are significantly reduced as compared with those of control specimens. This is contributed to the strengthening schemes which limited shear cracking of joint cores. However, shear distortions of strengthened specimens under low axial load increase significantly at the advanced stage of loading. In contrast, shear strains of strengthened specimens under high axial load vary slightly during the test. Presence of high axial load has beneficial effect on reducing shear distortions of strengthened beam-column joints. Influence of skeletal reinforcements on shear distortion is only assessed for specimens under low axial load. Specimen EJS4 with diagonal skeletal reinforcement exhibits slightly higher shear distortion as compared with specimen EJS3 with grid skeletal reinforcements. Both arrangements of skeletal reinforcements have similar effect on limiting shear distortion. Generally, the proposed strengthening method using ferrocement composites with skeletal reinforcements is effective for improving shear deformation of beam-column joints without transverse reinforcements.

3.7 Joint shear strength

Shear strength of beam-column joints is estimated to investigate the effectiveness of the proposed strengthening method for beam-column joints. It is noted that shear strengths are estimated at ultimate state for control specimens and at critical cracking for strengthened specimens (except specimen EJS1 failed in beam shear). Based on force equilibrium of a free-body joint, horizontal shear force at mid-height of exterior beam-column joint can be computed by Eq. (2)

$$V_{jh} = T - V_c \tag{2}$$

where T is the tension force of beam reinforcements and V_c is the column shear force. Tension force in the beam reinforcements is determined based on sectional analysis of beam. As shown in Fig. 5, beam shear force V_b is calculated using Eq. (3) which considered influence of P-Δ effect

$$V_b = V_c \frac{l_c}{l_b} + P \frac{\Delta}{l_b} \tag{3}$$

where P is the axial force; Δ is the horizontal displacement at upper column; l_c and l_b are the lengths of column and beam, respectively. Joint shear stress is equal to joint shear force divided by effective area of joint which is defined by ACI-ASCE 352 (2002). Joint shear strength for each specimen is shown in Table 4.

Joint shear strengths are enhanced for strengthened specimens under both high and low axial loads. For specimens under high axial load, joint shear strengths are increased by 15.9% and 5.5% for specimens EJS1 and EJS2, respectively. Joint shear strengths are increased by 5.8% and 6.8% for specimens EJS3 and EJS4, respectively. However, enhancement ratio on joint shear strength is smaller than that on peak horizontal load for each specimen. Joint shear strengths are not

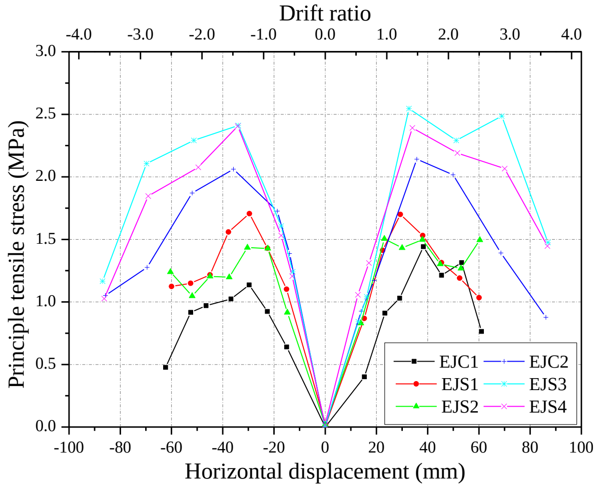

Fig. 16 Comparison of principal tensile stresses in joint cores

proportion to peak horizontal loads due to the influence of P-Δ effect. Moreover, joint shear strength is less susceptible to axial load. Joint shear strength is slightly decreased by 2.6% for control specimen as axial load increases. Similar decrease is found for strengthened specimen with diagonal skeletal reinforcements. However, joint shear strength increases for strengthened specimens with grid skeletal reinforcements when increasing axial load. It can be verified by the failure mode which is shifted from the joint to the beam.

3.8 Principal tensile stress

Nominal principal tensile stress in a beam-column joint is computed by Eq. (4) (Karayannis and Sirkelis 2008)

$$\sigma_t = \frac{\sigma_p}{2} + \sqrt{\frac{\sigma_p^2}{4} + v_{jh}^2} \tag{4}$$

where σ_t and σ_p are the principal tensile stress and axial compression stress in the joint, respectively; and v_{jh} is the joint shear stress. Fig.16 shows principal tensile stress developed in the joint against horizontal displacement for specimens under high and low axial loads. Maximum principal tensile stresses of strengthened specimens are higher than those of control specimens. It reflects the contribution of ferrocement for enhancing the tensile/shear strength of beam-column joints. Specimens under low axial load achieve higher principal tensile stresses as compared with those under high axial load. Increasing the axial load on column reduces the principal tensile stress in the joint.

3.9 Damage indices

Damage level of beam-column joints is examined using Park and Ang’s model as applied in beam-column joints (Karayannis *et al.* 2008). This model comprises a linear combination of ultimate displacement and dissipated energy as shown in Eq. (5)

$$D = \frac{\delta_M}{\delta_u} + \frac{\beta}{Q_y \delta_u} \int dE \tag{5}$$

where δ_M is the maximum deflection attained during seismic loading; δ_u is the ultimate deflection capacity under monotonic load; β is a model parameter that depends on shear force, axial force, amount of longitudinal and confinement reinforcements; Q_y is the calculated yield strength; and dE is the incremental dissipated energy. In this model, δ_M, Q_y and dE are determined based on the experimental results. δ_u consists of deformations contributed from beam, columns and joint. Monotonic deformations of beam and columns are calculated based on the empirical formula for the evaluation of ultimate drift ratio according to CEN Eurocode 8 (2004)

$$\delta_u = \frac{1}{\gamma_{el}} 0.016 \times \left(0.3^{P^*}\right) \left[\frac{\max(0.01;\omega^{'})}{\max(0.01;\omega)} f_c \right]^{0.225} \left(L^*\right)^{0.35} \times 25^{\left(\alpha \rho_s \frac{f_{yt}}{f_c}\right)} (1.25)^{100\rho_d} \tag{6}$$

where γ_{el} is equal to 1.0 in this study; P^* is the axial load index and is equal to $P/bhf_c^{'}$; b and h are width and height of the cross-section, respectively; $\omega^{'}$ and ω are the ratio of tension and compression reinforcements, respectively; f_c is the concrete strength; L^* is the shear span index and is equal to M/Vh; ρ_s is the transverse reinforcement ratio and is equal to A_{sx}/bs_h; s_h is the spacing of transverse reinforcements; f_{yt} is the yield strength of transverse reinforcement; ρ_d is the diagonal reinforcement ratio; and α is the confinement effectiveness factor derived from the following equation (Karayannis *et al.* 2008).

$$\alpha = \left(1 - \frac{s_h}{2b_0}\right)\left(1 - \frac{s_h}{2h_0}\right)\left(1 - \frac{\sum b_i^2}{6b_0 h_0}\right) \tag{7}$$

where b_0 and h_0 are the dimensions of confined concrete core to the centerline of transverse reinforcements; and b_i is the centerline spacing of longitudinal reinforcements (index by i) laterally restrained by a stirrup corner or a cross-tie along the perimeter of the cross-section. In respect of joint shear deformation capacity, it is determined based on experimental results. The model

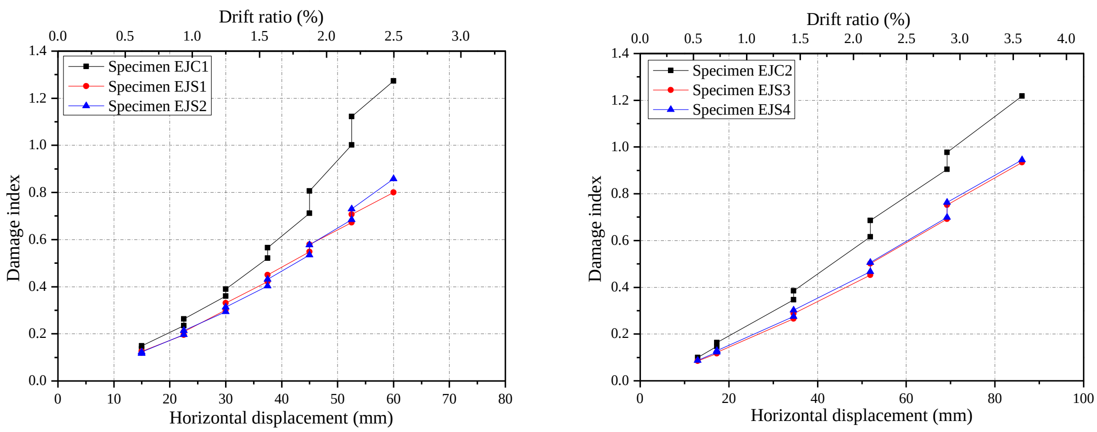

(a) (b)

Fig. 17 Comparison of damage indices for the specimens under (a) high axial load and (b) low axial load parameter β is taken to be 0.25 for the control specimens and 0.15 for the strengthened specimens as adopted in Li *et al.* (2013).

Fig. 17 plots damage indices against horizontal displacement for the specimens under high and low axial loads. Strengthened specimens show lower damage indices at each drift ratio as compared with corresponding control specimens. The proposed strengthening method is effective to upgrade beam-column joints. Strengthening schemes with different skeletal reinforcements barely affect damage level of strengthened specimens under respective axial loads. Comparing reduction in damage indices of specimens under high and low axial loads, strengthening method is more effective for the specimens under high axial load.

4. Discussion

4.1 Effect of axial load

Test results indicate that the increase in axial load has detrimental effect on peak horizontal load. For instance, increasing axial load from $0.2f_c^{'}A_g$ to $0.4f_c^{'}A_g$, peak horizontal load of control specimen is reduced by 17.5%. Similarly, peak horizontal loads are also decreased for the strengthened specimens with the same strengthening scheme when increasing axial load. Further, effect of axial load on joint shear strength is not significant. Joint shear strength of beam-column joint without transverse reinforcements is decreased by 2.6% when increasing axial load. However, joint shear strength is increased for strengthened specimens with grid skeletal reinforcements. On the other hand, joint shear strength of specimen EJS2 under high axial load is slightly lower than that of specimen EJS4 under low axial load.

Under the same deformation demand (i.e., same drift ratio), beam-column joints under high axial load exhibit higher energy dissipation as compared with that under low axial load. However, specimens under low axial load achieve higher drift ratio and have larger cumulative energy dissipation at final stage of loading. Except specimen EJS1 which failed in beam shear, all strengthened specimens under both high and low axial loads show similar improvement in energy dissipation. Initial stiffness of control specimens under both high and low axial loads is similar. After strengthening, enhancement in stiffness is higher for strengthened specimens under high axial load. However, stiffness degrades more rapidly for the specimens under high axial load. Generally, high axial load has beneficial effect for energy dissipation and stiffness at initial stage of loading. Subsequently, high axial load is detrimental for energy dissipation and stiffness degradation.

Shear distortion of beam-column joints is also significantly affected by axial load. As the increase in stiffness, joint shear distortions for specimens under high axial load are smaller than that of specimens under low axial load, especially at advanced stage of loading. This is attributed to that high axial load suppresses joint cracking through confinement. It indicates that high axial load is beneficial for reducing joint shear deformation.

4.2 Effect of skeletal reinforcements

Effect of skeletal reinforcements in ferrocement composites is estimated through comparing seismic performance of strengthened specimens under the same axial load. Use of U-shaped skeletal reinforcements in scheme *A* is effective for preventing formation of critical section at interface. It reduces strain penetration from longitudinal reinforcement into the joints. It is desirable to have more skeletal reinforcements in ferrocement in scheme *A* to allow formation of plastic hinge away from beam-column interface. Comparing with specimens with diagonal skeletal reinforcements, specimens with grid skeletal reinforcements exhibit slightly higher peak horizontal load but almost the same energy dissipation and stiffness (Fig. 11). Generally, both strengthening schemes with different skeletal reinforcements in ferrocement composites are effective for strengthening beam-column joints under both high and low axial loads.

4.3 Prediction of joint shear strength

Ferrocement-strengthened specimens are subjected to critical cracking within the joint. A method for calculating shear strength of strengthened specimens is proposed by summing up shear forces contributed from original joint core and ferrocement composites using Eq. (8).

$$V_n = V_{jc} + V_f \tag{8}$$

where V_n is the nominal shear capacity of ferrocement-strengthened beam-column joint. V_{jc} and V_f are the shear forces taking by original joint core and ferrocement composite, respectively.

Shear strength of original joint core can be computed using Eq. (9) as suggested in ACI-ASCE 352 (2002).

$$V_{jc} = \gamma\sqrt{f_c^{'}}b_j h_c \tag{9}$$

where γ is the joint shear strength factor; b_j is the effective width of joint and is determined according to ACI-ASCE 352 (2002). h_c is the depth of the column along the horizontal direction. For beam-column joint with transverse reinforcement less than 0.3% volumetric ratio, γ is specified to be 0.5 in ASCE/SEI 41 (2007). This factor underestimates shear strength of the joint, even for that without transverse reinforcement (Li *et al.* 2013 and Park and Mosalam 2013). According to shear strengths of control specimens in this study, a new factor 0.75 is recommended in the prediction.

Table 5 Comparison of tested and predicted joint shear forces for specimens

Spe.	(1) $V_{jh.exp}$ (kN)	Calculated shear force of components				(6) $V_{jh.cal}$ (kN) (2)+(4)	(7) $V_{jh.cal}$ (kN) (3)+(4)	(8) $V_{jh.cal}$ (kN) (3)+(5)	(9) $V_{jh.exp}$/ $V_{jh.cal}$ (1)/(6)	(10) $V_{jh.exp}$/ $V_{jh.cal}$ (1)/(7)	(11) $V_{jh.exp}$/ $V_{jh.cal}$ (1)/(8)
		(2) Concr. (0.5)#	(3) Concr. (0.75)*	(4) Frro. (Eq.6)	(5) Frro. (Eq.7)						
EJC1	400.9	268.1	402.1	0.0	0.0	268.1	402.1	402.1	1.50	1.00	1.00
EJC2	405.5	261.9	392.9	0.0	0.0	261.9	392.9	392.9	1.55	1.03	1.03
EJS1	464.8	209.6	314.4	158.6	122.1	368.2	473.0	436.5	1.26	0.98	1.06
EJS2	428.9	212.6	318.8	124.7	99.9	337.2	443.5	418.7	1.27	0.97	1.02
EJS3	447.1	213.3	320.0	139.1	111.9	352.5	459.1	431.9	1.27	0.97	1.04
EJS4	438.7	207.4	311.1	126.5	100.9	333.9	437.6	412.0	1.31	1.00	1.06
								Mean:	1.36	0.99	1.04

#γ=0.5 as recommended by ASCE/SEI 41 (2007)
*γ=0.75 as suggested in this study

In this study, ferrocement composites with skeletal reinforcements experienced critical cracking but without ultimate failure. Contribution of ferrocement to shear strength is estimated using two formulas suggested by Mansur and Ong (1987) and Desayi and Nandakumar (1995). The former has been proposed for assessing diagonal cracking strength of ferrocement in Eq. (10) while the latter is a best-fit equation developed for ferrocement with web shear cracking in Eq. (11). The latter also considers the influence of wire mesh and skeletal reinforcements on shear strength.

$$V_f = 6.8(f_m^{'}\rho_m \frac{h_c}{a})^{0.75}(b_f h_c) \tag{10}$$

$$V_f = 1.257\frac{b_f h_c \sqrt{f_m}}{\sqrt{(a/h_c)^2+1}}[0.234 + 40.11(\rho_m + \rho_{sr})\sin\theta] \tag{11}$$

where b_f is the thickness of ferrocement. a and h_c are the shear span and depth of ferrocement panel; f_m and $f_m^{'}$ are the cube and cylinder mortar strengths, respectively; ρ_m and ρ_{sr} are the longitudinal ratio of wire mesh and skeletal reinforcements in ferrocement. θ is the inclination of the crack with the longitudinal axis of the joint.

Shear forces of beam-column joints with and without strengthening are predicted using Eqs. (8) to (11) and are compared with the test results in Table 5. Shear strength of beam-column joints without transverse reinforcement is conservatively underestimated when joint shear strength factor is 0.5 in ASCE/SEI 41 (2007). Shear strength factor is recommended to be 0.75 giving the best prediction. Shear strengths of ferrocement predicted using both Eqs. (6) and (7) are almost similar. Generally, shear forces of ferrocement-strengthened beam-column joints is well predicted while using Eqs. (8) to (11).

5. Conclusions

An experimental investigation was performed to evaluate the effectiveness of using ferrocement to strengthen non-seismically designed RC exterior beam-column joints. Influences of axial load and skeletal reinforcements in ferrocement were assessed experimentally. Based on the observations and test results, the following conclusions can be drawn.

• RC exterior beam-column joints without transverse reinforcements exhibit joint shear failure with diagonal cracks.

• The proposed strengthening method using ferrocement composites is effective for suppressing joint shear failure and reducing the damage in the joint. It is verified by that joint shear distortions of strengthened specimens are significantly reduced as compared with that of control specimens.

• Application of ferrocement is effective to enhance the seismic performance of beam-column joints in terms of peak horizontal load, energy dissipation, stiffness and joint shear strength.

• For control specimens, high axial load is detrimental with respect to peak horizontal load. After strengthening, specimens EJS1 and EJS2 with higher axial load show improvement in peak horizontal load as compared with specimens EJS3 and EJS4 with low axial load. Further, high axial load is beneficial for enhancing energy dissipation and stiffness at the initial stage of loading but is detrimental at the advanced stage of loading.

• Use of grid skeletal reinforcements in ferrocement exhibits more improvement in seismic performance as compared with the use of diagonal skeletal reinforcements.

• Shear strength of ferrocement-strengthened beam-column joints can be predicted using the proposed method that superposes the shear contributions from original joint core and ferrocement composites.

Acknowledgements

The authors are grateful to the financial support from The Hong Kong Polytechnic University and the Research Grants Council of Hong Kong (RGC No: PolyU 5206/08E). The authors would like to thank the technical assistances provided by Structural Engineering Research Laboratory and Concrete Technology Laboratory of The Hong Kong Polytechnic University.

References

ACI-ASCE 352. (2002), *Recommendations for design of beam-column connections in monolithic reinforced concrete structures*, Joint ACI-ASCE Committee 352, Farmington Hills, MI.

Akguzel, U. and Pampanin, S. (2010), "Effects of variation of axial load and bidirectional loading on seismic performance of GFRP retrofitted reinforced concrete exterior beam-column joints", *J. Compos. Constr*., **14**(1), 94-104.

Alcocer, S.M. and Jirsa, J.O. (1993), "Strength of reinforced-concrete frame connections rehabilitated by jacketing", *ACI Struct. J*., **90**(3), 249-261.

Al-Salloum, Y.A., Siddiqui, N.A., Elsanadedy, H.M., Abadel, A.A. and Aqel, M.A. (2011), "Textile-reinforced mortar versus FRP as strengthening material for seismically deficient RC beam-column joints", *J. Compos. Constr*., **15**(6), 920-933.

Al-Salloum, Y.A., Alsayed, S.H., Almusallam, T.H. and Siddiqui, N.A. (2010), "Seismic response of FRP-upgraded exterior RC beam-column joints", *J. Compos. Constr*., **14**(2), 195-208.

Antonopoulos, C.P. and Triantafillou, T.C. (2003), "Experimental investigation of FRP-strengthened RC beam-column joints", *J. Compos. Constr.*, **7**(1), 39-49.

ASCE/SEI 41. (2007), *Seismic rehabilitation of existing buildings*, ASCE/SEI 41-06, Reston, VA.

Asha, P. and Sundararajan, R. (2014), "Experimental and numerical studies on seismic behaviour of exterior beam-column joints", *Comput. Concrete*, **13**(2), 221-234.

Babaeidarabad, S., Loreto, G. and Nanni, A. (2014), "Flexural strengthening of RC beams with an externally bonded fabric-reinforced cementitious matrix", *J. Compos. Constr*., **18**(5), 04014009.

CEN Eurocode 8 (2004), *Design of structures for earthquake resistance - part 3: assessment and retrofitting of buildings*, Brussels, Belgium.

Chalioris, C.E., Favvata, M.J. and Karayannis, C.G. (2008), "Reinforced concrete beam-column joints with crossed inclined bars under cyclic deformations", *Earthq. Eng. Struct. Dyn*., **37**(6), 881-897.

Copconcrete (1987), *Code of practice for the structural use of concrte-1987*, Buildings and Lands Department, Hong Kong.

Costa, R.J.T., Gomes, F.C.T., Providencia, P.M.M.P. and Dias, A.M.P.G. (2013), "Influence of shear deformation of exterior beam-column joints on the quasi-static behavior of RC framed structures", *Comput. Concrete*, **12**(4), 393-411.

Desayi, P. and Nandakumar, N. (1995), "A semi-empirical approach to predict shear strength of ferrocement", *Cement Concrete Compos*., **17**(3), 207-218.

Ehsani, M.R. and Wight, J.K. (1985), "Effect of transverse beams and slab on behavior of reinforced concrete beam-to-column connections", *ACI J. Proc*., **82**(2), 188-195.

Ghobarah, A., Aziz, T.S. and Biddah, A. (1997), "Rehabilitation of reinforced concrete frame connections

using corrugated steel jacketing", *ACI Struct. J.*, **94**(3), 283-294.
Ghobarah, A. and Said, A. (2002), "Shear strengthening of beam-column joints", *Eng. Struct*., **24**(7), 881-888.
Hassan, W.M. and Moehle, J.P. (2012), "Experimental assessment of seismic vulnerability of corner beam-column joints in older concrete buildings", *Proceeding of 15WCEE*, Lisbon, Portugal.
Hakuto, S., Park, R. and Tanaka, H. (2000), "Seismic load tests on interior and exterior beam-column joints with substandard reinforcing details", *ACI Struct. J*., **97**(1), 11-25.
Ho, I.F.Y., Lam, E.S.S., Wu, B. and Wang, Y.Y. (2013), "Monotonic behavior of reinforced concrete columns confined with high-performance ferrocement", *J. Struct. Eng*., ASCE, **139**(4), 574-583.
Kam, W.Y., Pampanin, S. and Elwood, K. (2011), "Seismic performance of reinforced concrete buildings in the 22 February Christchurch (Lyttelton) earthquake", *Bull. NZ. Soc. Earthq. Eng*., **44**(4), 239-278.
Kannan, P., Sivakumar, S. and Bindhu, K.R. (2013), "Seismic strengthening of exterior RC beam-column joints by advanced ferrocement jacketing", *Int. J. Innovat. Res. Sci*., *Eng. Tech*., **2**(1), 53-58.
Karayannis, C.G., Chalioris, C.E. and Sirkelis, G.M. (2008), "Local retrofit of exterior RC beam-column joints using thin RC jackets - an experimental study", *Earthq. Eng. Struct. Dyn.*, **37**(5), 727-746.
Karayannis, C.G. and Sirkelis, G.M. (2008), "Strengthening and rehabilitation of RC beam-column joints using carbon-FRP jacketing and epoxy resin injection", *Earthq. Eng. Struct. Dyn*., **37**(5), 769-790.
Kazemi, M.T. and Morshed, R. (2005), "Seismic shear strengthening of R/C columns with ferrocement jacket", *Cement Concrete Compos*., **27**(7-8), 834-842.
Li, B. and Chua, H.Y.G. (2009), "Seismic performance of strengthened reinforced concrete beam-column joints using FRP composites", *J. Struct. Eng*., ASCE, **135**(10), 1177-1190.
Li, B., Lam, E.S.S., Wu, B. and Wang, Y.Y. (2013), "Experimental investigation on reinforced concrete interior beam-column joints rehabilitated by ferrocement jackets", *Eng. Struct*., **56**, 897-909.
Mansur, M.A. and Ong, K.C.G. (1987), "Shear-strength of ferrocement beams", *ACI Struct. J*., **84**(1), 10-17.
Mourad, S.M. and Shannag, M.J. (2012), "Repair and strengthening of reinforced concrete square columns using ferrocement jackets", *Cement Concrete Compos*., **34**(2), 288-294.
Naaman, A.E. (2000), *Ferrocement and Laminated Cementitious Composites*, Techno Press 3000.
Pantelides, C.P., Okahashi, Y. and Reaveley, L.D. (2008), "Seismic rehabilitation of reinforced concrete frame interior beam-column joints with FRP composites", *J. Compos. Constr*., **12**(4), 435-445.
Paramasivam, P., Lim, C.T.E. and Ong, K.C.G. (1998), "Strengthening of RC beams with ferrocement laminates", *Cement Concrete Compos*., **20**(1), 53-65.
Park, S. and Mosalam, K.M. (2013), "Experimental investigation of nonductile RC corner beam-column joints with floor slabs", *J. Struct. Eng*., ASCE, **139**(1), 1-14.
Prota, A., Nanni, A., Manfredi, G. and Cosenza, E. (2004), "Selective upgrade of underdesigned reinforced beam-column joints using carbon fiber-reinforced concrete", *ACI Struct. J*., **101**(5), 699-707.
Rajagopal, S., Prabavathy, S. and Kang, T.H.K. (2014), "Seismic behavior evaluation of exterior beam-column joints with headed or hooked bars using nonlinear finite element analysis", *Earthq. Struct.*, **7**(5), 861-875.
Ravichandran, K. and Jeyasehar, C.A. (2012), "Seismic retrofitting of exterior beam column joint using ferrocement", *Int. J. Eng. Appl. Sci*., **4**(2), 35-58.
Sezen, H. (2012), "Repair and strengthening of reinforced concrete beam-column joints with fiber-reinforced polymer composites", *J. Compos. Constr*., **16**(5), 499-506.
Shannag, M.J. and Alhassan, M.A. (2005), "Seismic upgrade of interior beam-column subassemblages with high-performance fiber-reinforced concrete jackets", *ACI Struct. J*., **102**(1), 131-138.
Sheela, S. and Geetha, B.A. (2012), "Studies on the performance of RC beam-column joints strengthened using different composite materials", *J. Inst. Eng. (India)*, *Series A*, **93**(1), 63-71.
Su, R.K.L. and Wong, S.M. (2007), "A survey on axial load ratios of structural walls in medium-rise residential buildings in Hong Kong", *HKIE Trans*., **14**(3), 40-46.

Takiguchi, K. and Abdullah. (2001), "Shear strengthening of reinforced concrete columns using ferrocement jacket", *ACI Struct. J.*, **98**(5), 696-704.
Tsonos, A.D.G. (2010), "Performance enhancement of R/C building columns and beam-column joints through shotcrete jacketing", *Eng. Struct.*, **32**(3), 726-740.

CC